

**Utility of natural and artificial geochemical tracers for leakage monitoring and quantification during an offshore controlled CO<sub>2</sub> release experiment**

**Supplementary Material**

Anita Flohr<sup>1\*</sup>, Juerg M. Matter<sup>1</sup>, Rachael H. James<sup>1</sup>, Kevin Saw<sup>2</sup>, Robin Brown<sup>2</sup>, Jonas Gros<sup>3</sup>, Stephanie Flude<sup>4</sup>, Christopher Day<sup>4</sup>, Kate Peel<sup>2</sup>, Douglas Connelly<sup>2</sup>, Christopher R. Pearce<sup>2</sup>, James A. Strong<sup>2</sup>, Anna Lichtschlag<sup>2</sup>, Darren J. Hillegonds<sup>4</sup>, Christopher J. Ballentine<sup>4</sup>, Rebecca L. Tyne<sup>4</sup>

<sup>1</sup> School of Ocean and Earth Science, National Oceanography Centre Southampton, University of Southampton Waterfront Campus, European Way, Southampton SO14 3ZH, UK

<sup>2</sup> National Oceanography Centre, European Way, Southampton SO14 3ZH, UK

<sup>3</sup> GEOMAR Helmholtz Centre for Ocean Research Kiel, Wischhofstr. 1-3, 24148 Kiel, Germany

<sup>4</sup> University of Oxford, Department of Earth Sciences, South Parks Road, Oxford OX1 3AN, UK

\*Corresponding author:

Anita Flohr (anita.flohr@noc.ac.uk) (<https://orcid.org/0000-0002-5018-5379>). Now at: National Oceanography Centre, European Way, Southampton, SO14 3ZH Southampton, UK

## S1 – Gas analysis of CO<sub>2</sub>, C<sub>3</sub>F<sub>8</sub>, SF<sub>6</sub>, CH<sub>4</sub>, C<sub>4</sub>F<sub>10</sub>

A flow-through Fourier-Transmission Infra-Red (FT-IR) analyser (*atmosFIR*, Protea Ltd. UK) (Figure 1) was used to measure the molar fractions of CO<sub>2</sub>, SF<sub>6</sub>, C<sub>3</sub>F<sub>8</sub> and CH<sub>4</sub> in the gas samples. The FT-IR was equipped with a custom-made sample injection system allowing reference gases to be injected. The gas bubble sampler (GBS) was connected to a regulator to reduce the outlet pressure to ~0.7 bar above atmospheric pressure. The gas then passed through a water trap (magnesium perchlorate (Mg(ClO<sub>4</sub>)<sub>2</sub>), a temperature logger (Lascar Electronics) and the sampling port before entering the analyser at 0.2 mL min<sup>-1</sup>. Prior to every measurement of a gas sample, the gas line was flushed with nitrogen (N<sub>2</sub>) to determine the background followed by flushing with a secondary calibration gas (BOC check standard, Table 1) (both at a pressure of 0.7 bar and a flow of 0.2 mL min<sup>-1</sup>) containing 32 ppmv of perfluorobutane (C<sub>4</sub>F<sub>10</sub>). The sample line was then flushed with the gas sample. Once the C<sub>4</sub>F<sub>10</sub> concentration had returned to background values, the gas line was considered to be fully flushed with the sample gas and was verified by stable CO<sub>2</sub>, CH<sub>4</sub>, C<sub>3</sub>F<sub>8</sub> and SF<sub>6</sub> concentrations reported by the analyser. The analyser performed and averaged 10 scans of FT-IR spectra per minute. The amount of sample gas in the GBS was usually enough to provide between 6-10 min of stable sample gas measurements. The standard deviation ( $\pm 1\sigma$ ) reported here for the individual tracer gas concentrations refers to the standard deviation of 6-10 spectral measurements performed on the same gas sample and is a measure of analytical reproducibility of the gas measurements. The relative standard deviation (RSD) of C<sub>3</sub>F<sub>8</sub> measurements ranged from 0.4 to 18.74 %, for SF<sub>6</sub> from 0.08 to 2.01 % and for CH<sub>4</sub> from 0.16 to 1.38 % (n=26). High RSDs of C<sub>3</sub>F<sub>8</sub> and SF<sub>6</sub> were related to concentrations lower than the optimal performance concentrations of the FT-IR.

The sampling port on the FT-IR instrument also allowed the collection of discrete sub-samples of the gas for later analysis of  $\delta^{13}\text{C}_{\text{CO}_2}$ ,  $\delta^{18}\text{O}_{\text{CO}_2}$  and Kr back onshore. Discrete gas samples were retrieved from the sampling port using gas tight syringes (Hamilton; needle diameter 0.3 mm) and were injected into pre-evacuated 12 mL Exetainers® with double wadded septa (Labco). The syringes were flushed before each sampling using a 150 mL gas sampling tube (Lenz) that was constantly flushed with N<sub>2</sub>. Discrete samples were retrieved for later isotopic analysis of  $\delta^{13}\text{C}_{\text{CO}_2}$ ,  $\delta^{18}\text{O}_{\text{CO}_2}$  and Kr concentration. To avoid suction of atmospheric air after the injection process, the Exetainers® were over-pressured (filled with 25 mL of gas). For

storage, silicone sealant (Dow Corning 734, multi-purpose one component silicone sealant) was applied to the top of the septum to seal the puncture. The gas samples were stored at room temperature.



Figure 1 Onboard gas analysis. a) Gas analyser used for on board analysis of  $\text{CO}_2$ ,  $\text{C}_3\text{F}_8$ ,  $\text{SF}_6$  and  $\text{CH}_4$ . b) Injection system of the gas analyser. The red circle indicates the sampling port for retrieving discrete gas samples.

Table 1 List of certified reference gases (primary reference gases) used for calibration.

Supplier	Certificate No	Certified					Uncertainty (%)
		$\text{C}_3\text{F}_8$	$\text{SF}_6$	Kr	Balance	$\text{C}_4\text{F}_{10}$	
BOC	18/013264	0.2 %	2.8 %	50.36 %	$\text{CO}_2$		$\leq 5$
BOC	18/013600	54.5 ppmv	52.3 ppmv	98.5 ppmv	$\text{CO}_2$		$\leq 5$
CK	2766	0.4 ppmv	5 ppmv	90.0 ppmv	$\text{CO}_2$		$\pm 2$
BOC	19/012174				$\text{N}_2$	32 ppmv	$\leq 5$

## S2 – Krypton quantification

Krypton concentrations were measured using the MiniRUEDI portable mass spectrometer (Brennwald et al., 2016) and calibrated against custom-made reference gases. For a given mass to charge ration ( $m/z$ ) the peak intensity is proportional to the partial pressure of the relevant gas species, which is a function of the concentration of the gas species of interest in the gas, and the total gas pressure in the sample. Thus, the quantification of Kr concentrations required the samples to be run against a reference gas of both, (i) similar composition (i.e.,  $\text{CO}_2$  as balance gas) and (ii) the same pressure as the sample. Calibration reference gases were created by mixing pure industrial grade  $\text{CO}_2$  gas (BOC) with defined volumes of Kr-rich certified reference gases (Table 1). Five sets of reference gases were created, providing Kr

concentrations of 45 ppm, 90 ppm, 261 ppm, 504 ppm, and 1506 ppm. Exetainers® for calibration gas measurements were prepared in the same way as Exetainers® in the field used for samples gas measurements, i.e., by injecting 25 mL of sample gas at ambient air pressure into a pre-evacuated 12 mL Exetainer®. This suite of reference gases was characterised using the MiniRUEDI and the data were used to create a calibration curve correlating measured intensity at  $m/z$  84 with the known concentration of total Kr in the reference gases. This calibration curve was used to select the most appropriate reference gas to calibrate samples against.

Gas consumption during the MiniRUEDI analyses was  $0.06 \text{ mL min}^{-1}$  (Brennwald et al., 2016). Typical analysis times were 10-15 minutes. This means that up to 7.5 % of the sample was consumed during analysis. As the Exetainers® are rigid containers, this means that the pressure in the Exetainer®, and therefore the measured intensity, decreased over time. To minimise errors introduced by this, a methodology for analysis was designed to ensure that all samples and reference gases were treated in exactly the same way and that sample consumption was consistent between samples and reference gases.

Each Exetainer® was analysed in two stages. First, an initial characterisation phase, lasting 17.5 minutes, where the Exetainer® was attached to one of the MiniRuedi's sampling inlet ports and mass scans were taken across  $m/z$  ranges of interest, to identify the gas species present and make a rough assessment as to the likely concentration. Second, a single analysis was carried out, measuring  $m/z$  28 ( $\text{N}_2$ ), 44 ( $\text{CO}_2$ ), 84 (Kr), and 86 (Kr) on the Faraday detector and  $m/z$  84 (Kr), and 86 (Kr) on the electron multiplier detector. Five cycles of measurements were made using the Faraday cup and a gate time of 1.0 seconds. Ten cycles of measurements were made using the electron multiplier detector and a gate time of 4.8 seconds. Each analysis purged the instrument with the sample gas for 140 seconds.

Sample analysis proceeded as follows. An Exetainer® containing sample gas was attached to an inlet port on the MiniRuedi and characterised using the above described mass scan routine. The approximate intensity at  $m/z = 84$  was compared to the calibration curve described above and used to select the most appropriate reference gas, which was attached to a second inlet port. After 17.5 minutes the inlet port was switched to that of the reference gas and the 17.5 minute characterisation phase was carried out. Immediately afterwards, a single analysis was carried out on the reference gas. Once the reference gas analysis was complete, a single analysis was carried out on the sample gas.

Spectrometer blanks were analysed one to three times per day, along with measurements of ambient laboratory air to monitor spectrometer performance. Full system blanks were first

113 measured by analysing empty Exetainers®, but the low pressure in the Exetainers® inhibited  
 114 flow of gas into the mass spectrometer. Full system blanks for Kr measurements were estimated  
 115 by filling empty Exetainers with 25 mL of pure CO<sub>2</sub> and measuring the signal intensity at m/z  
 116 = 84. The contribution of the full system blank to the <sup>84</sup>Kr measurements ranges from less than  
 117 0.01 % for a gas sample with 1500 ppm Kr to ~3 % of the signal size for a gas sample with just  
 118 45 ppm Kr. This blank measurement is not the result of Kr present in the pure CO<sub>2</sub> or  
 119 Exetainers®, but instead represents an unknown contaminant (likely a fragment of a complex  
 120 organic molecule), present within the Exetainers®, with interfering peaks at m/z = 84 and m/z  
 121 = 86.

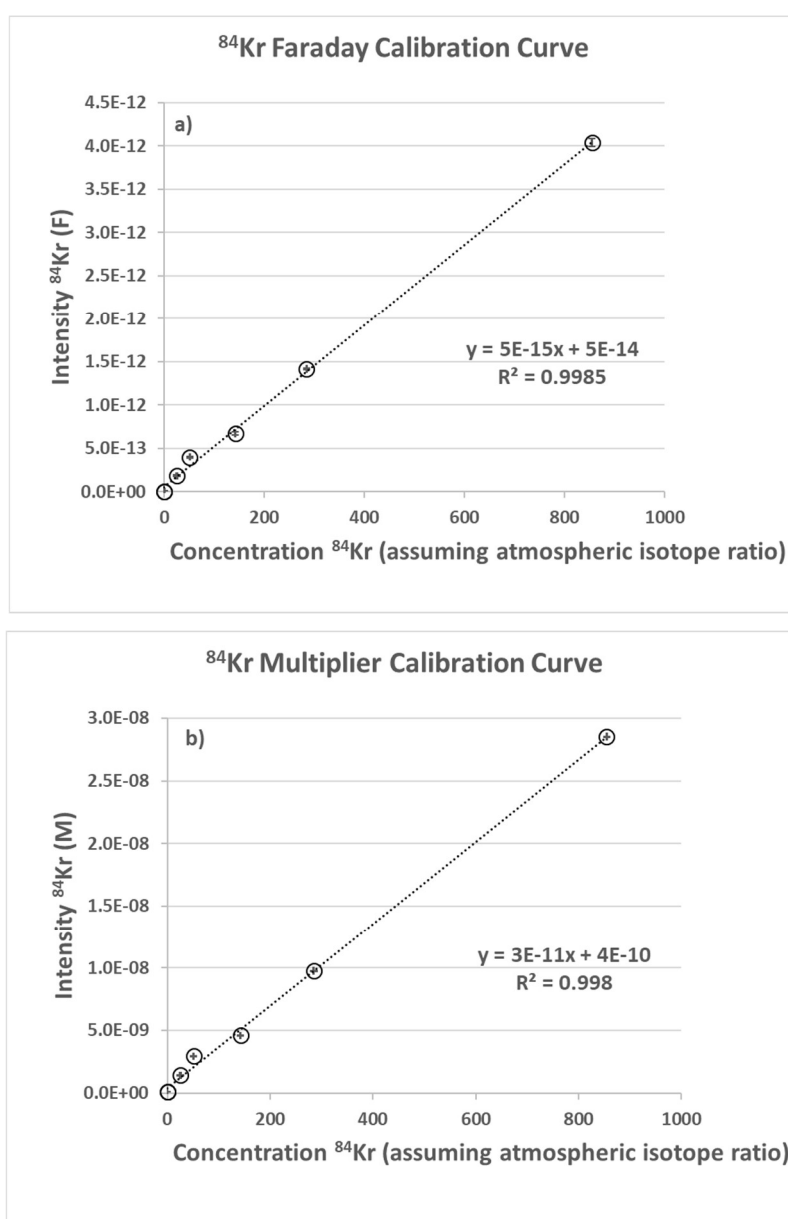


Figure 2 Calibration curves created from analyses of custom-made reference gases.

The main source of analytical uncertainty for the Kr measurements relates to differences in gas pressure inside the Exetainers® at the time of measurement. Potential sources of error include filling the exetainers with exactly the same amount of gas, and any small differences in sample consumption during the 17.5 minute characterisation phase of Exetainers® analysis. These uncertainties were assessed by preparing 3 Exetainers® of the 90 ppm Kr reference gas (which involves one injection step) and 3 Exetainers® of the 45 ppm Kr reference gas (which involves 3 injection steps to create the required concentration, and thus a greater risk of introducing errors). Each Exetainer® was characterised using the usual 17.5 minute procedure, and then one quantitative analysis carried out. The m/z peak intensities of the different Exetainers® were compared, and uncertainty estimated by calculating averages and standard deviations of the 90 ppm Kr and the 4 ppm Kr Exetainers®. Faraday measurements of m/z=84 and 86 gave higher relative errors compared to secondary electron multiplier measurements, due to the relatively low concentration and thus signal to noise, and these are not thought to represent the uncertainty in filling the Exetainers®. Relative percentage errors on CO<sub>2</sub> and Kr peaks range from 0.76 % to 2.58 %. To ensure we are not under-estimating the uncertainty of the measurements, we apply a RSD of 3 % to the true concentration of the reference gases. This uncertainty is propagated through all of the calculations and is incorporated in the final concentrations.

### S3 – Gas mixing system

Performance test runs of tracer injection under different CO<sub>2</sub> flow rates (24, 43, 86, 172, 286 kg d<sup>-1</sup>) and CO<sub>2</sub>:tracer injection ratios (12,500:1 and 10,000:1) prior to deployment on the seabed revealed fluctuations in tracer concentrations, especially at lower flow rates ( $\leq 29$  kg d<sup>-1</sup>). These test runs suggested that small pressure differences between tracer outlet pressure and CO<sub>2</sub> pressure impeded the supply of tracers into the main CO<sub>2</sub> gas stream, resulting in transient spikes in tracer concentrations, which levelled out at concentrations below the target concentration, i.e., C<sub>3</sub>F<sub>8</sub> concentrations were at ~30-40 % and SF<sub>6</sub> concentrations were at ~5-10 % of their expected concentration.

During the release experiment a total of 11 gas samples were retrieved from the sampling point at the gas rig. Similar to the performance runs prior to the experiment, the tracer concentrations in the injected CO<sub>2</sub> fluctuated significantly especially at low injection flow rates (6 and 14 kg d<sup>-1</sup>). Measured tracer concentrations were between ~20 to 6000 % of their expected concentration consistent with ranges observed during the onboard test. However, at higher

injection flow rates (86 and 143 kg d<sup>-1</sup>) tracer concentrations were closer to the expected values, ranging from 44 to 103 % of their expected concentration. Crucially, ratios of SF<sub>6</sub>:C<sub>3</sub>F<sub>8</sub>, Kr:SF<sub>6</sub> and Kr:C<sub>3</sub>F<sub>8</sub> stabilised close to their expected values, which provided confidence in the robustness of tracer injection at these higher flow rates. CH<sub>4</sub> was present in trace quantities of ~54 ppmv in the main CO<sub>2</sub> gas tanks which gradually decreased to ~33 ppmv over the course of the experiment. As CH<sub>4</sub> was pre-mixed with the CO<sub>2</sub> in the CO<sub>2</sub> tanks, the CO<sub>2</sub>:CH<sub>4</sub> ratio was nevertheless more constant than the CO<sub>2</sub>:C<sub>3</sub>F<sub>8</sub>, CO<sub>2</sub>:SF<sub>6</sub> and CO<sub>2</sub>:Kr ratio especially at low flow rates, so it could be utilised as a reference gas against which tracer gas results could be compared (Figure 3).

Although not conclusive, a possible cause of the tracer variability at lower flow rates was excessive pipe length between the tracer MFC and the mixing point. The two were connected by a 6 m length of flexible hose with an inside diameter of 6.35 mm with the tracer finally entering the main CO<sub>2</sub> flow via a 0.572 mm diameter orifice. The internal volume of this hose was ~190 mL. Given that the tracer MFC was metering gas at rates of fractions of millilitres per minute, any slight pressure differences between the main CO<sub>2</sub> line and the tracer flow line would affect the flow rate of tracer into the main CO<sub>2</sub> line. For example, when the main CO<sub>2</sub> flow rate was increased, a sudden pressure drop was observed at the tracer MFC outlet, P5 (Figure 3). This was most likely caused by the tracer orifice acting as a reverse pitot element. The only way the pressure in the tracer line can recover is by the introduction of new tracer gas into the line from the MFC which, by design, is metering at a very slow rate (0.01 to 0.28 in-situ mL min<sup>-1</sup> for 6 to 143 kg d<sup>-1</sup> overall release rate). The effect therefore is a reduced amount of tracer introduced to the main flow line. The tracer line pressure gradually recovers (as illustrated in Figure 3 c) but at an unacceptably slow rate. The gas mixing arrangement should be redesigned for future deployments to reduce the volume between the tracer MFC and the mixing point to an absolute minimum.

The impeded supply of tracers into the main CO<sub>2</sub> gas stream should in theory apply for all added tracers in the same way assuming that the tracer gas mixture was well mixed within the bladder accumulators. The fact that Kr concentrations in the final gas mixture were closer to the expected values than SF<sub>6</sub> and C<sub>3</sub>F<sub>8</sub> could be an indication of an effect of SF<sub>6</sub> and C<sub>3</sub>F<sub>8</sub> adsorption. The CO<sub>2</sub> storage and injection system was designed with minimum use of plastics and rubber elastomers and most of the parts used were made of stainless-steel. Since the CO<sub>2</sub> was by far the most reactive gas among the gases used, and is known to cause swelling of rubbers, the selection of plastic (PVC for flexible hose) and rubber-elastomer materials (e.g., Viton for the bladder accumulators, Parker-Hydrin for flexible hoses) (Figure 1, main paper)

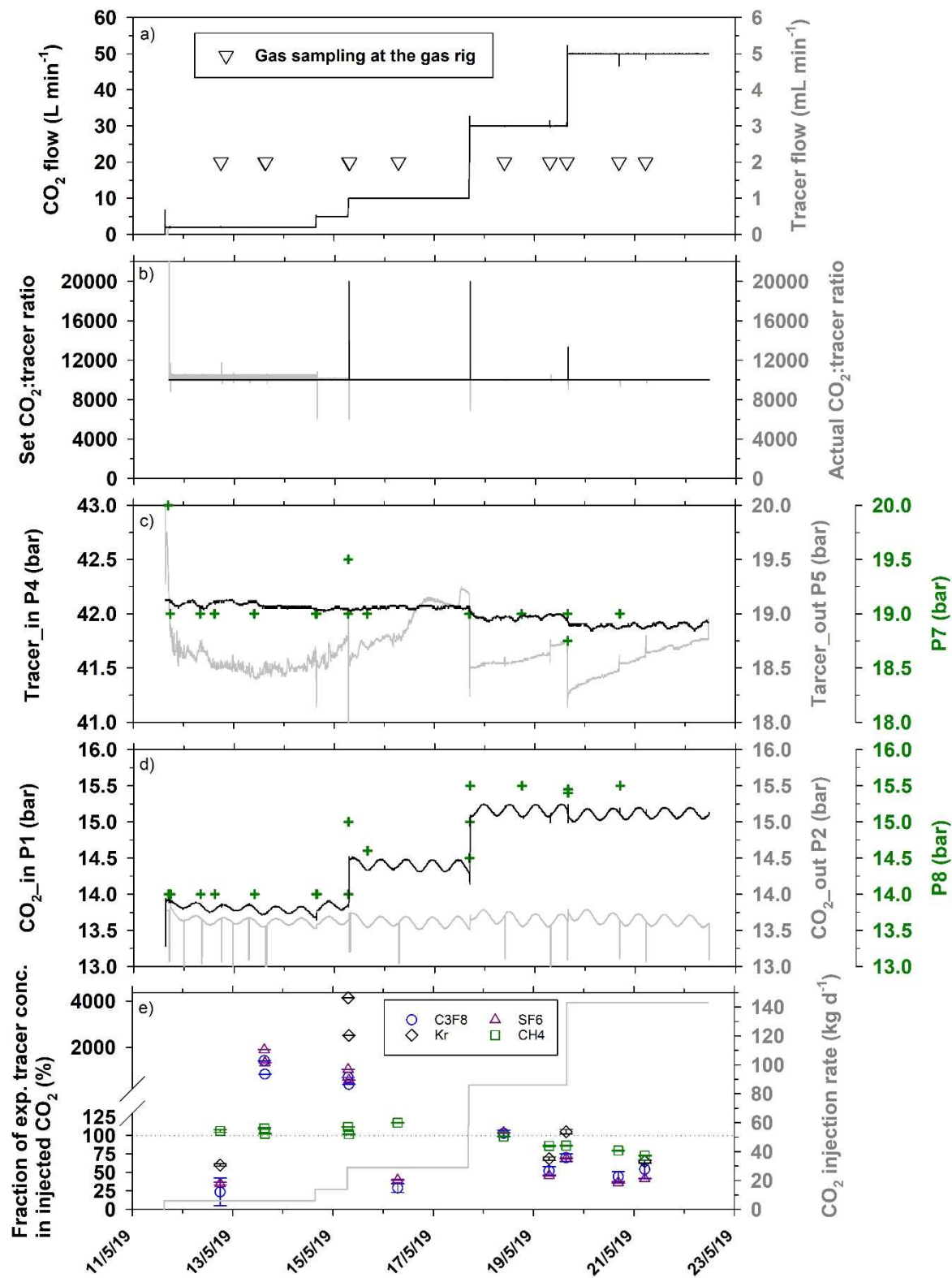
190 was mainly guided by assuring CO<sub>2</sub> compatibility. Tracer compatibility was checked but the  
191 available information was often very limited.

192

193

194





197 Figure 3 Output from the gas control unit over the period of the CO<sub>2</sub> release experiment. a)  
198 Measured CO<sub>2</sub> flow (left y-axis, L min<sup>-1</sup>) and measured tracer flow (right y-axis, hidden behind  
199 black line) (mL min<sup>-1</sup>). Triangles indicate when gas was sampled at the gas rig. b) Expected

(left y-axis) and measured CO<sub>2</sub>:tracer ratio (right y-axis). c) Tracer inlet pressure (left y-axis), tracer outlet pressure (right y-axis) and P7 (secondary right y-axis, green crosses) (all in bar). P7 is the pressure in the CO<sub>2</sub> gas line where the CO<sub>2</sub> and the tracer mixture were mixed (please also refer to the Fig. 1 in the main paper). d) Inlet pressure of mixed CO<sub>2</sub> (left y-axis) and outlet pressure of mixed CO<sub>2</sub> (right y-axis) (both in bar) and P8 (secondary right y-axis, green crosses). P8 is the pressure of the mixed CO<sub>2</sub> just before it enters the mass flow controller unit and thus P1 (please also refer to the Fig. 1 in the main paper). e) Temporal variability of tracer concentrations measured in discrete gas rig samples (left y-axis, % of expected concentration) throughout the release experiment. The respective CO<sub>2</sub> injection flow rates are indicated (right y-axis, kg d<sup>-1</sup>). The graphs show that the tracer outlet pressure (i) dropped when the flow rate was changed, (ii) gradually increased after those drops but did not stabilise throughout the experiment and (iii) was usually lower than P7, which was the pressure apparent in the CO<sub>2</sub> line into which the tracer was being mixed. It needs to be noted that P8, P7 were a dial gauge read via the ROV video so the accuracy of these values is lower.

214

## S4 – Composition of gas samples

Table 2 Composition of gas sampled from the CO<sub>2</sub> release system's sample point (rig), from the bubble streams (seep) above the seabed and from the same seep higher up in the water column (seep wc). Numbers in italic font have not been used for reported tracer-based calculations of CO<sub>2</sub> dissolution in porewater due to instability of the tracer injection.

ROV dive #	source	Date	Injection rate (kg d <sup>-1</sup> )	CO <sub>2</sub> (%)	RSD (%)	C <sub>3</sub> F <sub>8</sub> (ppm)	RSD (%)	SF <sub>6</sub> (ppm)	RSD (%)	Kr (ppm)	RSD (%)	CH <sub>4</sub> (ppm)	RSD (%)	δ <sup>13</sup> C <sub>CO2</sub> V-PDB (‰)	δ <sup>18</sup> O <sub>CO2</sub> V-SMOW (‰)
359	rig	12/05/19	6	97.75	1.11	<i>0.03</i>	<i>18.74</i>	<i>0.62</i>	<i>1.64</i>	<i>23.49</i>	<i>1.53</i>	48.32	1.83	19.15	34.10
359	seep	12/05/19	6	98.38	0.64	<i>0.14</i>	<i>2.43</i>	<i>3.67</i>	<i>0.80</i>	<i>413.69</i>	<i>1.60</i>	74.25	0.94	19.45	38.50
361 1	rig	13/05/19	6	97.86	0.84	<i>1.53</i>	<i>0.91</i>	<i>33.46</i>	<i>1.38</i>	<i>1879.49</i>	<i>4.02</i>	49.94	1.20	19.04	33.28
361 2	rig	13/05/19	6	98.44	0.44	<i>0.90</i>	<i>0.87</i>	<i>23.56</i>	<i>0.91</i>	<i>2204.85</i>	<i>2.92</i>	46.60	0.87	19.04	33.13
361	seep	13/05/19	6	97.00	0.74	<i>8.68</i>	<i>1.01</i>	<i>182.06</i>	<i>1.88</i>	<i>3329.81</i>	<i>3.58</i>	124.94	1.24	20.25	39.59
363 1	rig	15/05/19	29	98.89	0.28	<i>0.75</i>	<i>0.40</i>	<i>18.31</i>	<i>0.08</i>	<i>n.d.</i>	<i>n.d.</i>	50.81	0.33	19.04	34.08
363 2	rig	15/05/19	29	98.85	0.28	<i>0.42</i>	<i>0.71</i>	<i>10.20</i>	<i>0.15</i>	<i>1622.19</i>	<i>2.52</i>	46.34	0.36	19.04	33.80
363	seep	15/05/19	29	98.32	0.34	<i>0.22</i>	<i>1.95</i>	<i>5.52</i>	<i>0.36</i>	<i>983.19</i>	<i>1.21</i>	104.80	0.49	19.75	36.18
370	rig	18/05/19	86	99.29	0.38	0.11	4.16	1.83	0.41	58.23	2.17	44.94	0.54	19.04	33.45
370 1	seep	18/05/19	86	99.15	0.44	0.15	2.48	2.80	0.60	97.10	2.12	77.57	0.66	19.65	35.07
370 2	seep	18/05/19	86	99.02	0.44	0.17	2.87	3.10	0.62	111.52	2.96	79.41	0.45	19.75	35.00
372	rig	19/05/19	86	98.87	0.56	0.06	6.08	0.81	0.88	26.84	2.42	39.13	0.84	19.04	34.52
372	seep	19/05/19	86	99.22	0.28	0.16	3.07	2.76	0.34	91.74	2.94	80.88	0.39	19.85	35.53
372	seep wc	19/05/19	86	98.74	0.63	0.28	3.67	5.00	0.77	277.57	1.65	134.48	0.93	20.55	34.92
373	rig	19/05/19	86	97.11	0.42	0.08	5.18	1.22	0.56	41.14	2.98	39.33	0.62	19.04	33.73
373	seep*	19/05/19	86	98.82	0.52	0.14	4.86	2.55	0.62	91.73	1.76	70.56	0.75	19.85	35.12
373	seep wc*	19/05/19	86	97.41	0.25	0.29	0.71	5.32	0.27	321.06	2.42	139.08	0.27	20.65	35.21
376	rig	21/05/19	143	97.24	0.29	0.06	12.04	0.73	0.46	25.33	1.91	33.09	0.50	19.04	34.26
376	seep*	21/05/19	143	98.87	0.45	0.09	8.62	1.55	0.62	53.94	1.71	55.89	0.56	19.55	34.65
376	seep wc*	21/05/19	143	97.30	0.59	0.64	1.42	11.1	0.77	576.29	2.94	278.15	0.58	21.66	35.24

\* same seep sampled on consecutive days

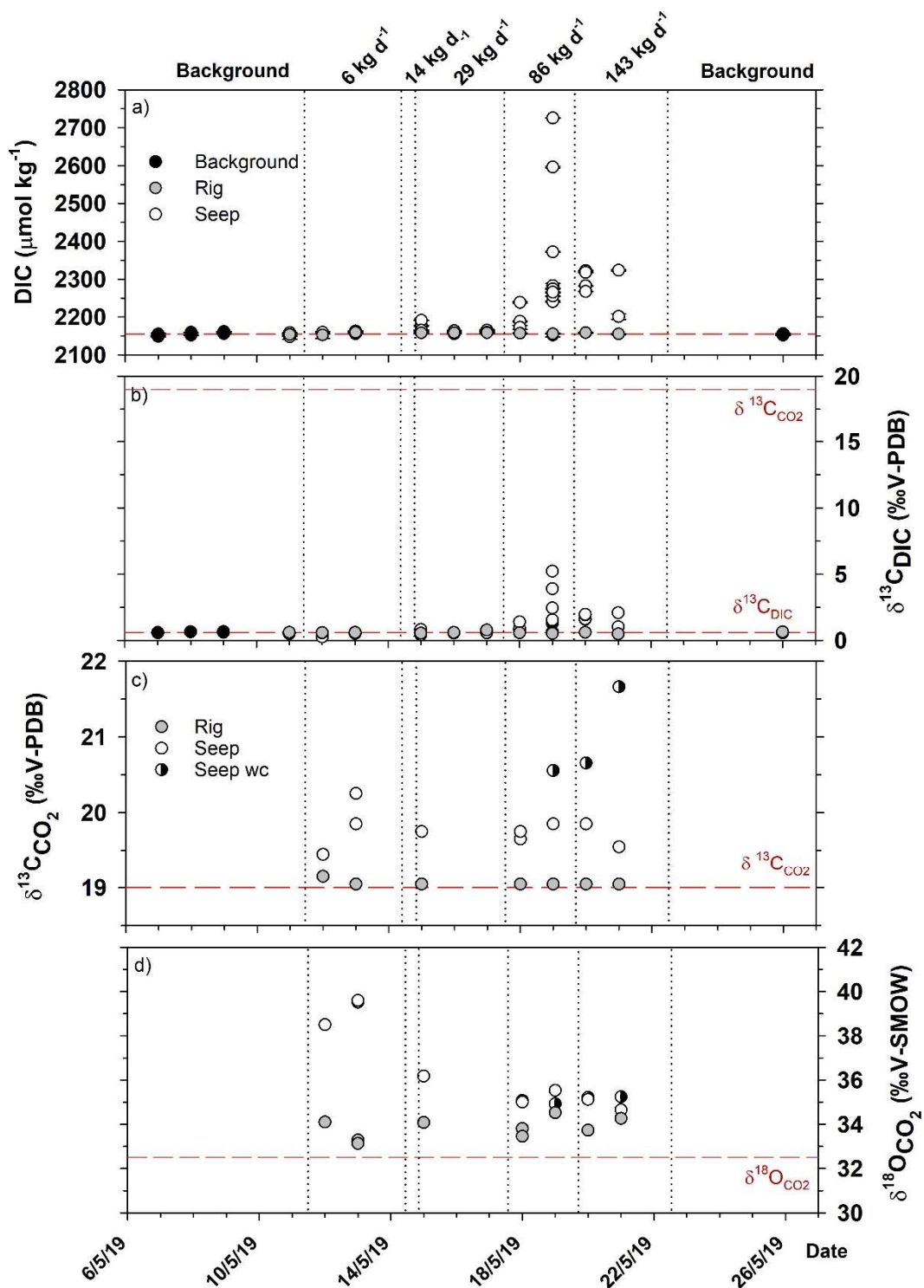


Figure 4 a) DIC and b)  $\delta^{13}\text{C}_{\text{DIC}}$  measured in water samples from before, during and after the injection of the  $\text{CO}_2$ -tracer mixture into the sub-seabed sediments. The water samples were taken away from the release side (background, rig) and above the bubble stream between 1.5-2.5 m above the seafloor (seep). c)  $\delta^{13}\text{C}_{\text{CO}_2}$  and d)  $\delta^{18}\text{O}_{\text{CO}_2}$  measured in gas samples from

the sample point at the gas rig (rig), from the seep close to the seabed (seep) and the same seep higher up in the water column (seep wc).

## S6 – Simulated evolution of $\delta^{13}\text{C}_{\text{CO}_2}$ and $\delta^{13}\text{C}_{\text{DIC}}$ as a function of aqueous $\text{CO}_2$ dissolution

The  $\text{CO}_2$  isotope dissolution from gas bubbles into ambient seawater was simulated using TAMOC, as described in another article of this issue (Gros et al., 2021). The model simulates the kinetics of mass transfer of the  $^{12}\text{C}$  and  $^{13}\text{C}$  isotopes of  $\text{CO}_2$  from dissolving gas bubbles into pore water. In these simulations, isotope fractionation is assumed to be driven by isotope differences in aqueous solubility and by isotope difference in diffusion coefficients in water, which together drive the rate of mass transfer of the isotopes into ambient seawater (Wanninkhof, 1985). This corresponds to a Rayleigh process. For the simulation (i) chemical properties of the  $^{13}\text{C}$  isotope were used (Jähne et al., 1987; Vogel et al., 1970), (ii) a source value of  $\delta^{13}\text{C}_{\text{CO}_2} = 19.04 \text{ ‰}$  (Section 3.2.1, main paper) was used, and (iii) it was assumed that the ambient seawater was depleted in  $\text{CO}_2$ . This simulation was verified by field data, i.e., by the change observed in  $\delta^{13}\text{C}_{\text{CO}_2}$  of seep gas samples versus  $\delta^{13}\text{C}_{\text{CO}_2}$  of seep gas samples at 0.9–2.7 masf (S4, Supplementary Material, Table 2), which confirms that the observed changes in  $\delta^{13}\text{C}_{\text{CO}_2}$  can be attributed to aqueous dissolution.

Here, the simulation was used to quantify  $\text{CO}_2$  dissolution in the sediment pore water (Figure 5). The observed change in isotopic composition from  $\delta^{13}\text{C}_{\text{CO}_2} = 19.04 \text{ ‰}$  for rig samples to 19.45 to 20.25 ‰ for seep samples indicates a  $\text{CO}_2$  dissolution into pore water of 22–53 % (Figure 5, Table 3). These estimates are slightly lower but in good agreement with  $\text{CH}_4$ -based estimates. Deviations between the  $\text{CH}_4$ -based and  $\delta^{13}\text{C}_{\text{CO}_2}$ -based estimates are likely caused by more complex in-situ conditions (e.g., saturated pore water, occurrence of carbonate dissolution) compared to the simplified assumptions mentioned above. To a first order, analyses of porewater  $\delta^{13}\text{C}_{\text{DIC}}$  are also consistent with  $\text{CH}_4$ -based estimates of dissolution of injected  $\text{CO}_2$  into sediment pore waters (Figure 6). Pore water  $\delta^{13}\text{C}_{\text{DIC}}$  evolves according to Rayleigh fractionation of C isotopes as the injected  $\text{CO}_2$  is converted to  $\text{HCO}_3^-$ . The model assumes (i) that all pore water DIC is  $\text{HCO}_3^-$ , and (ii) that the difference between  $\delta^{13}\text{C}_{\text{HCO}_3^-(\text{aq})}$  and  $\delta^{13}\text{C}_{\text{CO}_2(\text{g})}$  is +10 ‰ at 7 °C (Zhang et al., 1995).

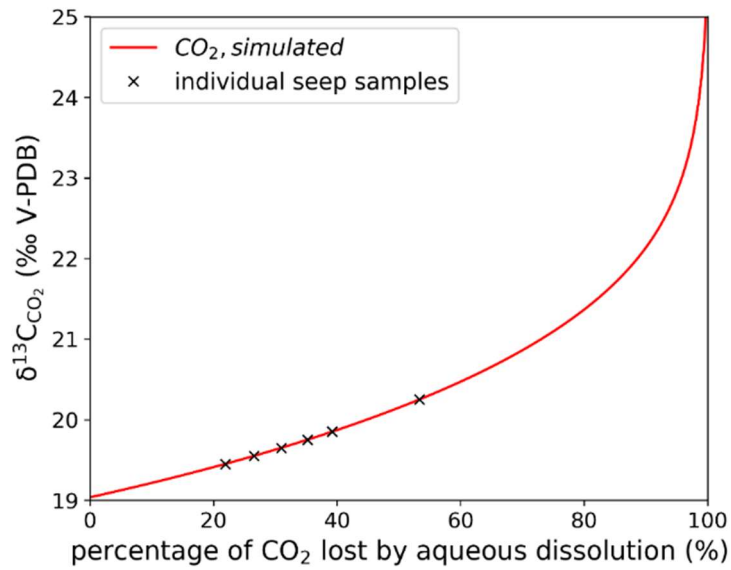


Figure 5 Predicted  $\delta^{13}\text{C}_{\text{CO}_2}$  as a function of the percentage of  $\text{CO}_2$  lost due to aqueous dissolution.

Table 3 Estimate of dissolved percentage of  $\text{CO}_2$  based on changes in  $\delta^{13}\text{C}_{\text{CO}_2}$  (relative to the average  $\delta^{13}\text{C}_{\text{CO}_2}$  of 19.04 ‰ measured in the rig gas samples).

ROV dive #	$\delta^{13}\text{C}_{\text{CO}_2}$ seep (‰ V-PDB)	Loss of $\text{CO}_2$ from injected $\text{CO}_2$ (%)
359	19.45	22
361	20.25	53
363	19.75	35
370 1	19.65	31
370 2	19.75	35
372	19.85	39
373	19.85	39
376	19.55	27

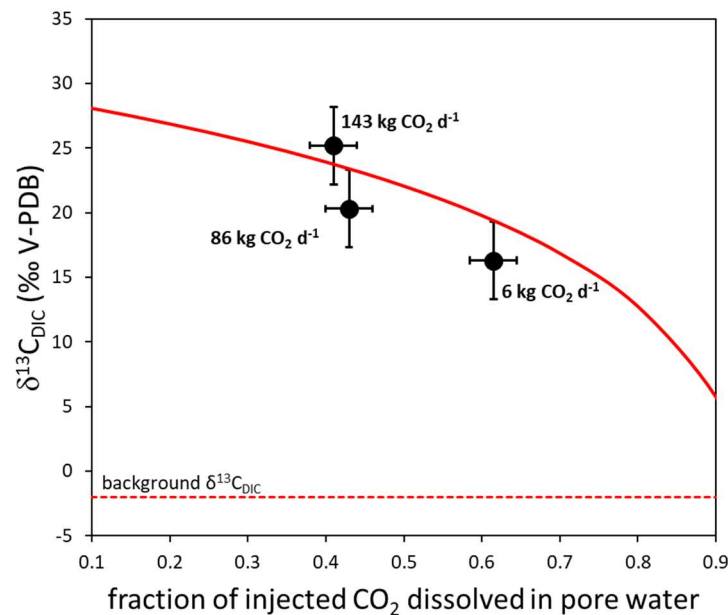


Figure 6 Modelled evolution of  $\delta^{13}\text{C}_{\text{DIC}}$  of sediment pore waters due to dissolution of the injected  $\text{CO}_2$  (solid red line). Black symbols show maximum measured pore water  $\delta^{13}\text{C}_{\text{DIC}}$  values (corrected for background DIC) for different  $\text{CO}_2$  injection rates as a function of the proportion of injected  $\text{CO}_2$  that dissolved obtained from  $\text{CH}_4$  tracer-based estimates (Table 3 in main paper). Error bars account for the uncertainty in the tracer-based estimates and variation in  $\delta^{13}\text{C}_{\text{DIC}}$  values in high DIC pore waters. Horizontal red dashed line shows the  $\delta^{13}\text{C}_{\text{DIC}}$  value of background seawater.

## References

- Brennwald, M. S., M., S., Oser, J., and Kipfer, R.: A Portable and Autonomous Mass Spectrometric System for On-Site Environmental Gas Analysis, *Environ. Sci. Technol.*, 50, 13455–13463, 10.1021/acs.est.6b03669, 2016.
- Gros, J., Schmidt, M., Linke, P., Dötsch, S., Triest, J., Martínez-Cabanas, M., Esposito, M., Dale, A. W., Sommer, S., Flohr, A., Fone, J., Bull, J. M., Roche, B., Strong, J. A., Saw, K., Brown, R., Koopmans, D., and Wallmann, K.: Quantification of dissolved  $\text{CO}_2$  plumes at the Goldeneye  $\text{CO}_2$ -release experiment, *International Journal of Greenhouse Gas Control*, 109, 103387, <https://doi.org/10.1016/j.ijggc.2021.103387>, 2021.
- Jähne, B., Heinz, G., and Dietrich, W.: Measurement of the diffusion coefficients of sparingly soluble gases in water, *Journal of Geophysical Research: Oceans*, 92, 10767-10776, <https://doi.org/10.1029/JC092iC10p10767>, 1987.
- Vogel, J. C., Groottes, P. M., and Mook, W. G.: Isotopic fractionation between gaseous and dissolved carbon dioxide, *Zeitschrift für Physik A Hadrons and nuclei*, 230, 225-238, 10.1007/BF01394688, 1970.
- Wanninkhof, R.: Kinetic fractionation of the carbon isotopes  $^{13}\text{C}$  and  $^{12}\text{C}$  during transfer of  $\text{CO}_2$  from air to seawater, *Tellus B*, 37B, 128-135, <https://doi.org/10.1111/j.1600-0889.1985.tb00061.x>, 1985.

293 Zhang, J., Quay, P. D., and Wilbur, D. O.: Carbon isotope fractionation during gas-water exchange and  
294 dissolution of CO<sub>2</sub>, *Geochimica et Cosmochimica Acta*, 59, 107-114,  
295 [https://doi.org/10.1016/0016-7037\(95\)91550-D](https://doi.org/10.1016/0016-7037(95)91550-D), 1995.  
296